Flow patterns of non-Newtonian nanofluid flow in cylindrical enclosure with rotating endwall: Effects of nanoparticles concentration

Haroun Ragueb[1*], *Hanan* Lamraoui[1], *Nabil* Himrane[1], *Belkacem* Manser[1] and *Kacem* Mansouri[1]

[1] Laboratory of Energy, Mechanics and Engineering, Faculty of Technology, University M'Hamed Bougara of Boumerdes (UMBB), Avenue of Independence, 35000, Boumerdes, Algeria.

Abstract. In this paper, a numerical study on the flow structure of non-Newtonian nanofluid in cylindrical enclosure with rotating end wall. The considered nanofluid, MWCNT-water, exhibits a strong power-law shear-thinning behavior with the increase in nanoparticles loading. The main focus in this study is the effect of nanoparticles concentration on the vortex breakdown phenomenon. The simulation results showed that adding a small amount of nanoparticle eliminate the vortex breakdown which is considered as a positive in mixing process. However, the increase in nanoparticles concentration as well as the enclosure aspect ratio promotes the apparition of secondary recirculation zone and stagnation zone.
Keywords. Rotating endwall, vortex breakdown, non-Newtonian nanofluid, MWCNT-water.

1 Introduction

The study of the flow topology in a closed cylindrical container with rotating endwall is an old problem, with important outcomes [1-3]. The problem encountered in this configuration is the apparition of vortex break down phenomena. Using laser-induced fluorescence technique, Escudier [4] visualized the steady swirling flow produced in cylindrical container completely full of fluid. It has been shown that the appearance of vortex breakdown depends mainly on two parameters: the Reynolds number and the aspect ratio of the container. Bohme et al. [5] carried out a numerical and experimental study on vortex breakdown in cylindrical vessel filled with a shear-thinning fluid. They showed that the flow patterns are highly dependent on the rheological behavior.

As most of fluids are non-Newtonian, and the particularity of this benchmark in understanding mixing process, several authors showed interest in investigating the flow topology produced with different kinds of fluid. Escudier and Cullen [6] studied the behavior of strong shear-thinning viscoelastic liquid using laser-induced fluorescence technique. Tamano et al. [7] investigated unsteady swirling flow of an aqueous polymer solution due to a rotating disk in a cylindrical casing. P-Morales and Zenit [8] carried out the problem of vortex rings in non-Newtonian shear-thinning liquids. They found that the vortex circulation decreases as the power-law index n decreases. Tchina et al. [9] studied numerically the burst formation and stagnation conditions within a flow driven by the rotation of the cover of vertical cylinder under the influence of density variation. The buoyancy effects are analyzed by applying a temperature gradient, between the ambient fluid and a small rod, placed in the center of the fixed disk.

Olsthoorn et al. [10] studied numerically the vortex dynamics in a non-Newtonian low viscosity fluid following Carreau rheological model. The steady-state mixed convection of Bingham fluids in a cylindrical enclosure with a heated rotating top cover has been numerically analyzed by Turan et al.[11]. In this work the authors examined the influence of different control parameters on the Nusselt number. Imoula et al. [12] studied numerically the effects of buoyant-thermocapillary convection on axisymmetric vortex flows driven by the disk rotation with free surface. The problem of mixing in flows dominated by bubble-type vortex breakdown has been examined numerically by Sharma and Sameen [13]. They found that in steady regime of the flow, the apparent non-axisymmetric features observed in experiments are artifacts of imperfections in experimental setups. Turan et al. [14] studied numerically the behavior of inelastic shear-thinning/shear-thickening fluids by applying power-law model of viscosity. In this work, the authors examined a large range of Reynolds, Richardson, Prandtl numbers and power-law index.

In this study, we investigate numerically the flow patterns of non-Newtonian nanofluid in cylindrical enclosure with rotating endwall. The main focus of this study is the effect of the nanoparticles concentration on vortex breakdown occurrence, as well the topology of the yielded flow.

*Corresponding author: h.ragueb@univ-boumerdes.dz

2 Analysis

2.1 Theoritical model

Consider a cylindrical enclosure with rotating bottom and filled with a shear-thinning nanofluid that obeys to the power-law model. The side wall and the top cover are assumed stationary, where the rotation axis (cylinder axis), correspond to the z-axis. The fluid physical properties are assumed to be constant, and the flow is assumed to be laminar, steady and axisymmetric. The fluid is kept at constant temperature, and the body forces are neglected. By considering these assumptions, the governing equations in the cylindrical coordinates (r, ϕ, z), can be written as follows:

1- Mass conservation equation

$$\frac{\partial u}{\partial r}+\frac{u}{r}+\frac{\partial w}{\partial z}=0 \tag{1}$$

2- Momentum conservation equations

$$\rho\left(u\frac{\partial u}{\partial r}-\frac{v^2}{r}+w\frac{\partial u}{\partial z}\right)=-\frac{\partial P}{\partial r}+\frac{\partial \tau_{zr}}{\partial z}+\frac{\partial \tau_{rr}}{\partial r}+\frac{\tau_{rr}-\tau_{\phi\phi}}{r} \tag{2}$$

$$\rho\left(u\frac{\partial v}{\partial r}-\frac{uv}{r}+w\frac{\partial v}{\partial z}\right)=\frac{\partial \tau_{r\phi}}{\partial r}+\frac{\partial \tau_{z\phi}}{\partial z}+\frac{2\tau_{r\phi}}{r} \tag{3}$$

$$\rho\left(u\frac{\partial w}{\partial r}+w\frac{\partial w}{\partial z}\right)=-\frac{\partial P}{\partial z}+\frac{1}{r}\frac{\partial\left(r\tau_{rz}\right)}{\partial r}+\frac{\partial \tau_{zz}}{\partial z} \tag{4}$$

3- Boundary conditions

$$\begin{cases} u=v=w=0,\ \{r=R\ ,z\in[0,H]\}\wedge\{r\in[0,R],z=H\} \\ u=w=0, v=\Omega R,\{r\in[0,R],z=0\} \\ \partial(.)/\partial r=0,\{r=0\ ,z\in[0,H]\} \\ \partial(.)/\partial\phi=0,\{r\in[0,R]\ ,z\in[0,H]\} \end{cases} \tag{5}$$

Here, u, v and w are the radial, tangential and the axial velocities with respect to directions r, ϕ and z respectively, ρ is the fluid density, P is the pressure and τ is the stress tensor.

According to the power-law model, the stress tensor τ_{ij} is expressed as the following [14]:

$$\tau_{ij}=\mu_a e_{ij}=K\left(\frac{1}{2}e_{kl}e_{kl}\right)^{\left(\frac{n-1}{2}\right)}e_{ij} \tag{6}$$

where the strain-rate tensor is given by:

$$e_{ij}=\left(\frac{\partial u_i}{\partial x_j}+\frac{\partial u_j}{\partial x_i}\right) \tag{7}$$

and the apparent viscosity is :

$$\mu_a=K\left(\frac{1}{2}e_{kl}e_{kl}\right)^{\left(\frac{n-1}{2}\right)} \tag{8}$$

Here, K is the consistency factor, and n is the rheological index. For n = 1, the fluid is considered Newtonian, for n < 1, the fluid has a shear-thinning behavior, while for n > 1, the fluid exhibit the shear-thickening behavior.

In this study, multi-walled carbon nanotubes (MWCNT) well dispersed in water and stabilized by adding 0.2 Wt.% of cationic chitosan, is considered as the working non-Newtonian nanofluid [15]. The particularity of this nanofluid is that it exhibits a strong power-law shear thinning behavior with respect to the nanotubes loading. The Table 1 presents the rheological indices as a function of the volumetric concentration, (φ), of nanoparticles measured experimentally.

Table 1. Power-law indices of MWCNT-water nanofluid [15, 16].

Wt.%	φ (Vol.%)	ρ (kg/m^3)	K (Pa.s^n)	n
0.0	0.00	997.10	0.0113	1.0000
1.0	0.48	1002.4	0.0167	0.8831
2.0	0.95	1007.6	0.2725	0.5078
3.0	1.43	1012.9	0.7711	0.3023

2.2 Numerical resolution, mesh stability and validation

The numerical simulations in the present study have been conducted using ANSYS-FLUENT-Academic Edition. The software solves Eqs. (1-5) with boundary conditions in Eq. (6) iteratively using the finite volume methodology [17]. The SIMPLEC scheme is used the pressure-velocity coupling, and PRESTO! for the pressure interpolation . For the discretization of the connective terms, the second order upwind scheme is used. The iterations are run until the residuals are all below the convergence criteria which is set equal to

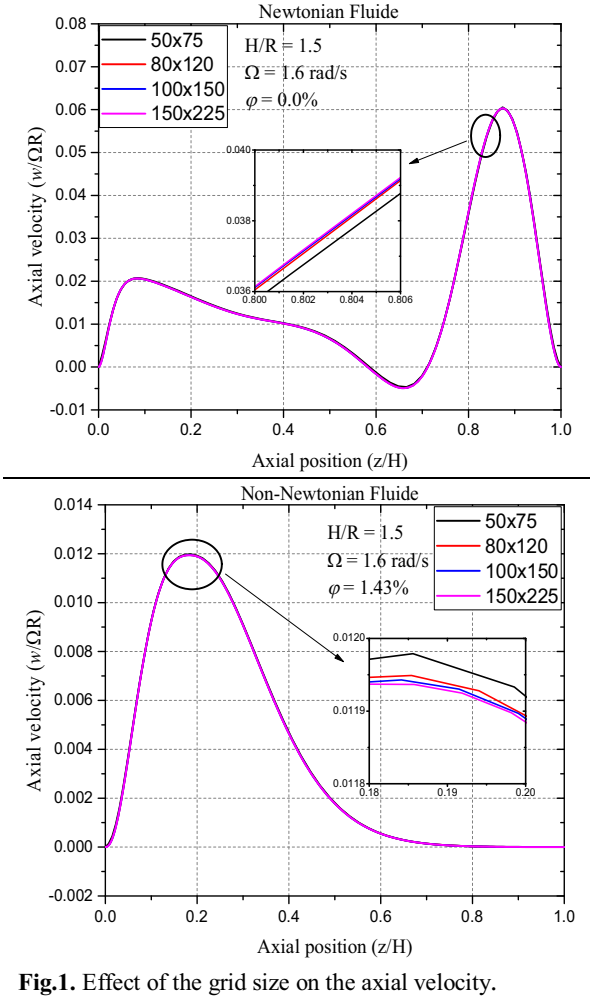

Fig.1. Effect of the grid size on the axial velocity.

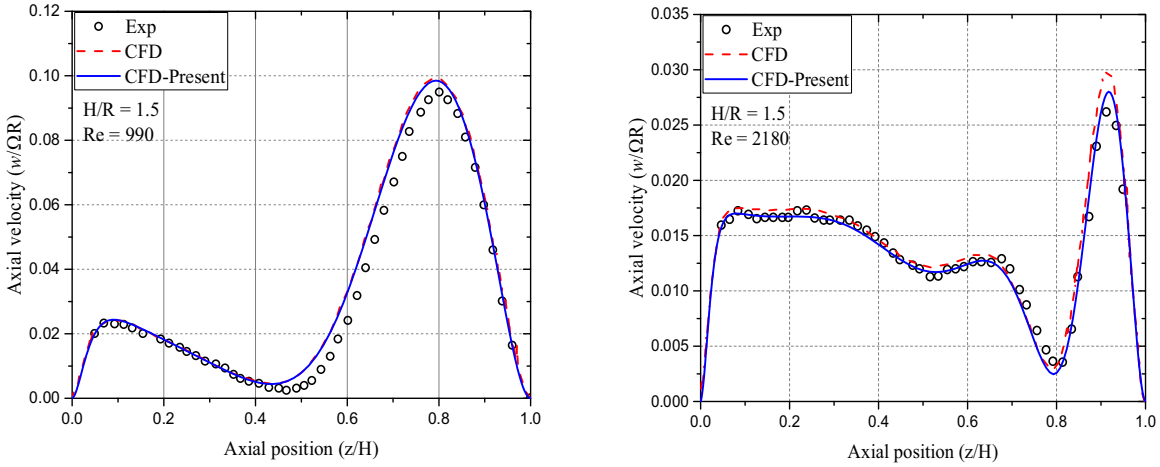

Fig. 2. Comparison of the axial velocity with literature (blue line: present study; dashed red line: CFD done by [18]; black circles: experiment done by [18]).

10^{-7}. The simulations are done in two dimensional, double precision, axisymmetric swirling mode

The geometry consists of a rectangle that represents a half of the meridional plan of the cylindrical enclosure. This rectangular is meshed using quadrilateral elements with smooth inflation near the walls and axis. Several grids with different sizes have been tested for the grid-independency for both cases of Newtonian and non-Newtonian behavior. The Fig. 1 represents the variation of the axial velocity scaled to the rotation velocity ($w/\Omega R$) along the scaled location at the central axis (z/H) for different grids. In this tests, the bottom wall is subject to a constant rotational velocity Ω = 1.6rad/s, and the cylindrical enclosure has a radius R = 10cm and a height H = 15cm, thus the aspect ratio H/R = 1.5. As it can be seen from the zoom in the figures, starting from a grid with 80×120 elements, the velocity is insensitive to the grid size for

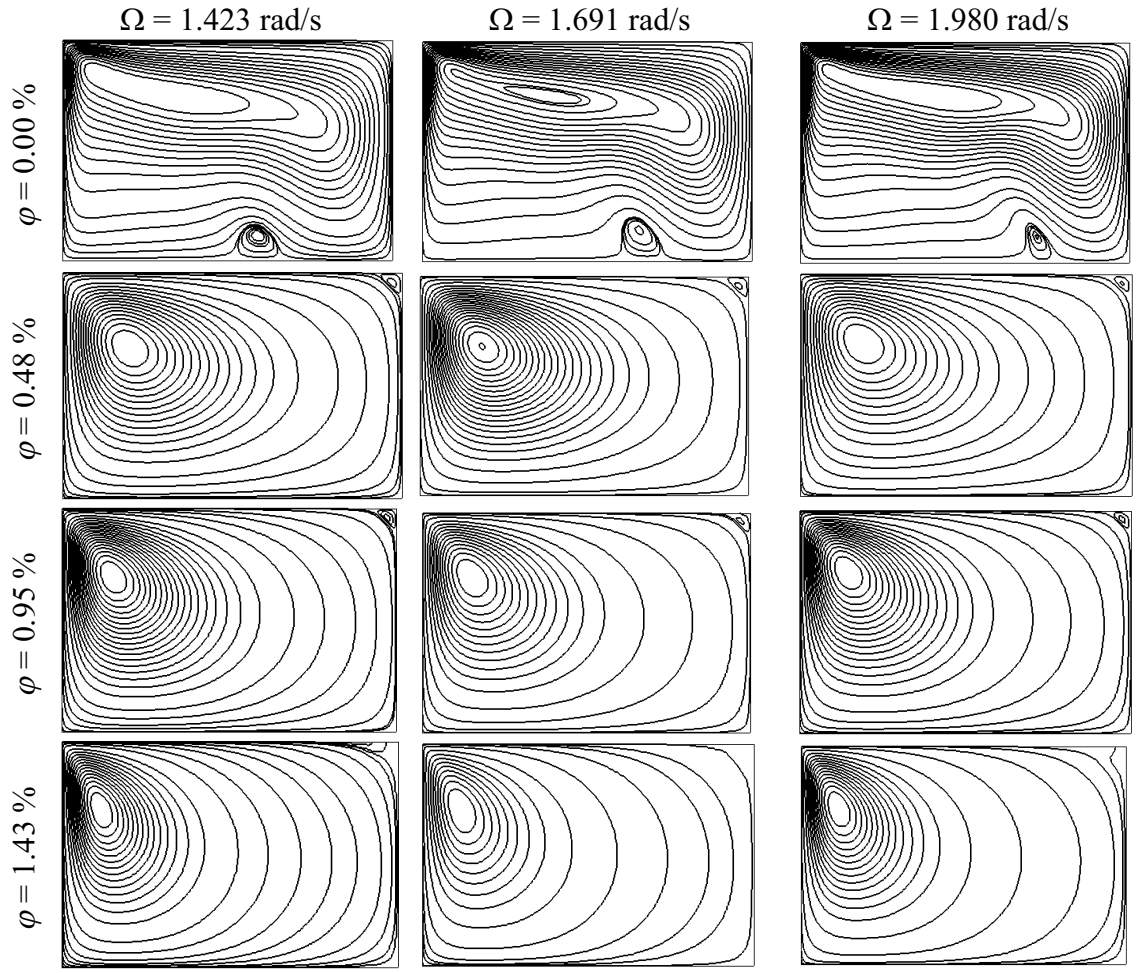

Fig. 3. Effect of the angular velocity and nanoparticles concentration on the flow pattern in a cylindrical enclosure with H/R = 1.5 (streamlines; axis is at the bottom edge, the rotating wall is the left edge).

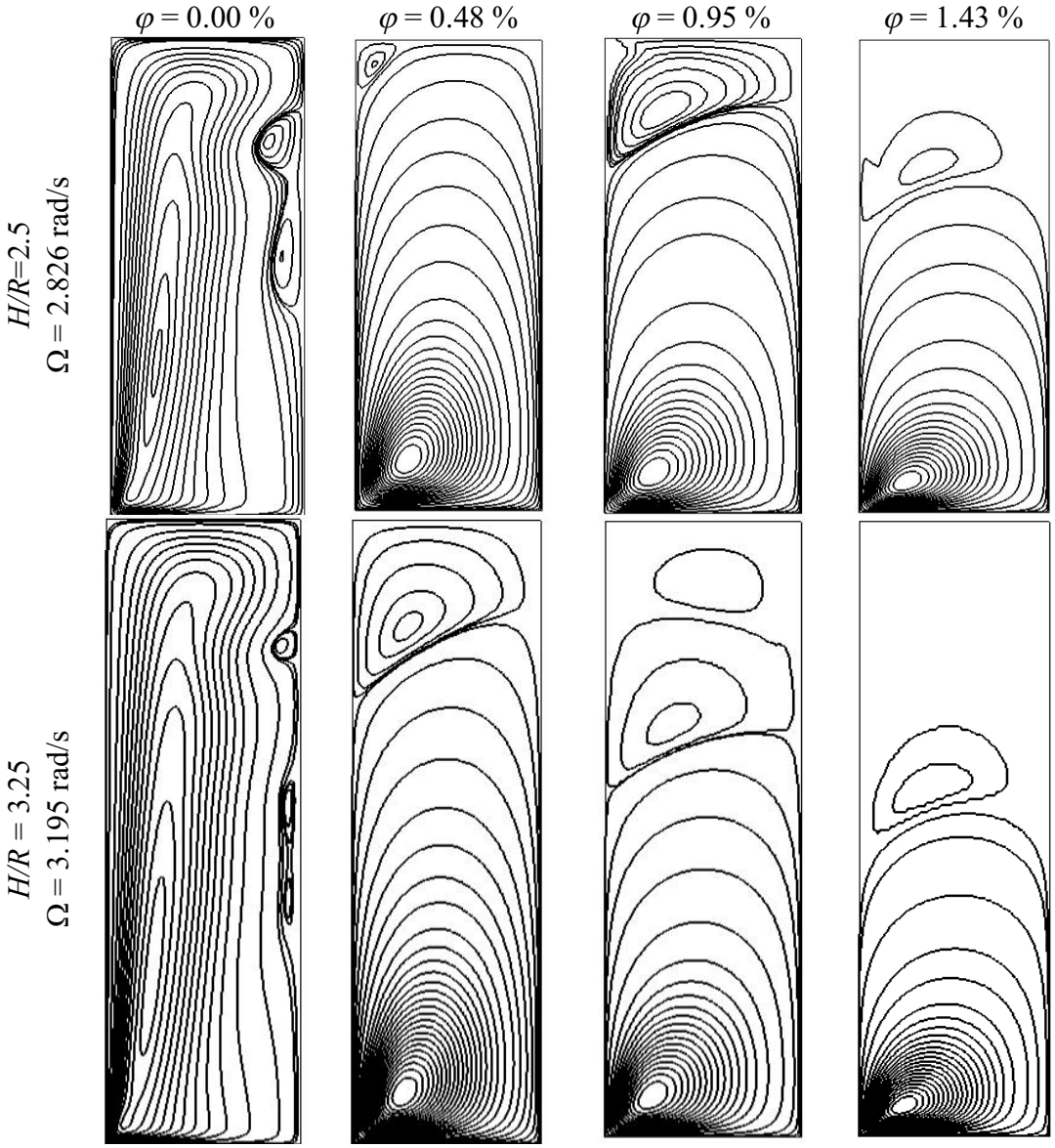

Fig. 4. Effect of the aspect ratio and the particle concentration on the flow topology (streamlines; axis is the right edge, the rotating wall is the bottom edge).

both fluids (Newtonian and non-Newtonian). In this study, the 100×150 grid is adopted and used in the remaining parts of this study. For the two other geometries with H/R = 2.5 and 3.25, it has been found that the results obtained with grids 100×250 and 100×325, respectively, are grid-independent (results not reported in this study).

The validity of the present simulations is checked by comparisons with literature. The Fig. 2 depicts a comparison based on the axial velocity along the z-axis in an enclosure with H/R = 1.5 and Re = 990 and 2180. As it can be seen, there is a good agreement with the present-CFD results and the CFD and experimental measurement of Yalagach and Salih [18], for both Reynolds number. In conclusion, the CFD model developed in this study can simulate the flow behavior with good adequacy to the realty.

3 Results and discussions

In the first set of simulations, a cylindrical enclosure with an aspect ratio H/R = 1.5 has been considered. To visualize the effect of adding nanoparticles, the angular velocity of the rotating bottom wall is set to a value where the vortex breakdown can be observed in the Newtonian fluid (in this case φ = 0%), then for the same angular velocity, the working Newtonian fluid is replaced with the non-Newtonian MWCNT-water nanofluid with φ = 0.48, 0.95 and 1.43%. In this set of simulations, we have considered three angular velocities, Ω = 1.423, 1.691 and 1.980 rad/s, that correspond to Newtonian Reynolds number, Re = 1256, 1492, 1747 respectively, where the vortex breakdown can be seen [4]. The streamlines in the meridional plan are presented in Fig. 3. The rotation axis in these figures is the horizontal bottom edge whereas the rotating bottom wall is the left vertical edge of each streamline-panel.

For the Newtonian case (φ = 0%) the phenomena of vortex breakdown can be observed for the three angular velocities. As the nanoparticles concentration increases, this phenomenon disappears. This can be attributed mainly the shear-thinning effects due to addition of nanoparticles. In this enclosure, the fluid flow in mainly a shear-driven flow, as the shear increases, the apparent viscosity of the nanofluid decreases especially near the axis, thus the disappearance of the vortex break-down. In addition, a cellular recirculation zone can be observed in the top right corner for φ = 0.48 and 0.95%, and disappears for

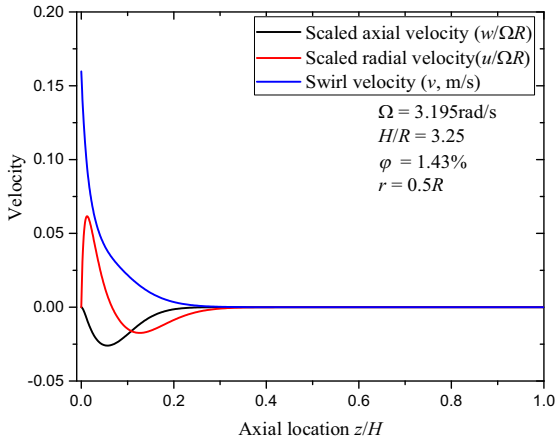

Fig. 5. Variation of velocity components along a vertical line parallel to the z-axis, located at $r = 0.5R$.

$\varphi = 1.43\%$. At this zone the shear rate is very low and decreases as φ increase, hence the apparent viscosity increases to the point where the flow is halted (a stagnation zone). This zone is emphasized with the increase in aspect ratio as we can see next.

In the second set of simulations, the aspect ratio has been increased to H/R = 2.5 and 3.25. The angular velocity is selected so that for the Newtonian fluid case, the vortex breakdown occurs with two bubbles for H/R = 2.5, and three bubble for H/R = 3.25 [4]. The results are depicted in Fig. 4, where the rotation axis is the vertical left edge and the rotating wall is the bottom edge. As it can be seen, the addition of nanoparticle eliminate the vortex breakdown, however, for low concentration (φ = 0.48%), a recirculation zone is developed near the top wall, and increases with the aspect ratio. As the nanoparticle concentration increases, a stagnation zone appears in the top region, and increases with the aspect ratio. The flow in this zone is halted.

The Fig. 5 depicts the velocity component (axial, radial and swirling) along a vertical line at r = 0.5R and parallel to the z-axis for the case of $\varphi = 1.43\%$ and H/R =3.25. The figure shows that as we move far from the rotation bottom, the velocity components decreases and tends to zero approximately at z/H=0.3. It can be explained by analyzing the Fig. 6 that depicts the variation of the strain rate and the apparent viscosity along this line. As we can see, near the rotating bottom, the strain rate is high thus the apparent viscosity is low due to shear thinning effect and fluid flows freely (velocity component have a significant value). As we move forward, the strain rate decreases which results in a significant increase in the apparent viscosity, hence the pumping effect created by the rotating bottom cannot reach this zone. From the practical view, this stagnation zone can be viewed as barriers in mixing equipments.

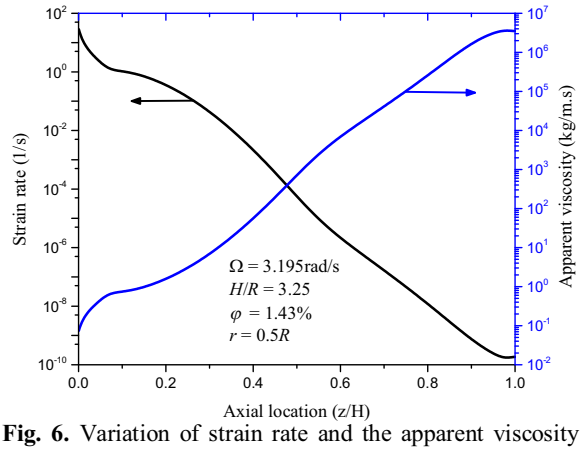

Fig. 6. Variation of strain rate and the apparent viscosity along a vertical line parallel to the z-axis and located at $r = 0.5R$.

4 Conclusions

In this study, a numerical investigation on the flow pattern of a non-Newtonian nanofluid, namely MWCNT-water, in a cylindrical enclosure with rotating end wall. The results show that the addition of nanoparticles eliminates the vortex breakdown phenomenon that is considered as barrier in mixing, due to the shear-thinning effect. However, a secondary recirculation zone forms near the opposite end wall, this zone increases with the increase of the aspect ratio for low nanoparticle concentration. As the last one increase, a stagnation zone is developed and it emphasizes with the increase of the aspect ratio. From the practical view point, this zones (recirculation and/or stagnation), can causes several problem in mixing process which can results in incorrect texture in the desired output product.

This work was supported by the ministry of higher education and scientific research of Algeria. Grant number : PRFU-A11N01UN350120220003.

References

1. Von-Kármán, T., ZAMM+Journal of Applied Mathematics and Mechanics/Zeitschrift für Angewandte Mathematik und Mechanik. **1**, 233(1921)
2. Bertelà, M., Computers & Fluids. **7**, 231(1979)
3. Escudier, M. and N. Zehnder, J Fluid Mech. **115**, 105(1982)
4. Escudier, M., Experiments in fluids. **2**, 189(1984)
5. Böhme, G., L. Rubart, and M. Stenger, Journal of Non-Newtonian Fluid Mechanics. **45**, 1(1992)
6. Escudier, M.P. and L.M. Cullen, Exp Therm Fluid Sci. **12**, 381(1996)
7. Tamano, S., et al., Phys Fluids. **19**, 023103(2007)
8. Palacios-Morales, C. and R. Zenit, Journal of Non-Newtonian Fluid Mechanics. **194**, 1(2013)
9. TCHINA, A., R. SACI, and R. GATIGNOL. *Stagnation conditions of a swirling flow in a cylinder under density variation*. in *21ème Congrès Français de Mécanique, 26 au 30 août 2013, Bordeaux, France(FR)*. 2013. AFM.
10. Olsthoorn, J., M. Stastna, and D. Steinmoeller, Phys Fluids. **26**, 013101(2014)

11. Turan, O., S. Yigit, and N. Chakraborty, International Journal of Heat and Mass Transfer. **108**, 1850(2017)
12. Imoula, M., S. Rachid, and F. Mustapha. *Effects of geometry and buoyant-thermocapillary convection on vortex flows in an open*. in *ICTEA: International Conference on Thermal Engineering*. 2018. Doha, Qatar.
13. Sharma, M. and A. Sameen, Physica Scripta. **94**, 054005(2019)
14. Turan, O., S. Yigit, and N. Chakraborty, Thermal Science and Engineering Progress. **18**, 100541(2020)
15. Phuoc, T.X., M. Massoudi, and R.-H. Chen, International Journal of Thermal Sciences. **50**, 12(2011)
16. Ragueb, H. and K. Mansouri, International Journal of Numerical Methods for Heat & Fluid Flow. **29**, 334(2019)
17. Patankar, S., *Numerical heat transfer and fluid flow*2018: Taylor & Francis.
18. Yalagach, A. and A. Salih, International Journal of Fluid Mechanics Research. **43**, (2016)